High-Temperature Sodium | Metal Chloride Storage Battery

Michael A. Vallance[*,1] and Ralph E. White[2]
[1]GE Global Research, [2]Department of Chemical Engineering, University of South Carolina
*One Research Circle, Niskayuna, NY 12309, vallance@crd.ge.com

Abstract: To understand the dynamics of electrochemical cycling, a high-temperature sodium | ferrous chloride storage cell was modeled in two dimensions. The positive electrode, micronized iron, ferrous chloride, and sodium chloride, impregnated with a molten-salt electrolyte, is represented as a continuum, using porous electrode theory. The cell can thusly be described using transport phenomena and heterogeneous reaction kinetics. The time-dependent solution shows that a reaction front, starting at the interface with the negative electrode, moves deeper into the positive electrode with increasing depth of discharge. Cell potential falls continuously as the discharge front moves deeper; Ohmic resistance in the porous electrode limits cell performance.

Keywords: electrochemical, storage, cell, sodium, ferrous, iron, chloride, FEM, transport.

1. Introduction

Sodium | metal chloride storage batteries provide high energy and power densities safely and reliably. These batteries are used in hybrid propulsion applications for rail, marine, industrial, and mass transit.

The battery cells, which operate at *ca* 300°C, use sodium-ion-conducting β″ alumina solid electrolyte (BASE) to separate the molten sodium negative electrode (anode) and the porous metal/metal chloride positive electrode (cathode). BASE is an insulator to electrons and other ions. The cathode is contained in a closed BASE tube, while the anode occupies the volume between the BASE tube and the steel case, which serves as the current collector for the negative electrode. In the present example, the cathode consists of iron, ferrous chloride ($FeCl_2$) and sodium chloride (NaCl) impregnated with molten-salt electrolyte sodium tetrachloroaluminate (STCA, $NaAlCl_4$). The cathode compartment includes a U-shaped metal-rod current collector (CC) and a reservoir for reserve STCA, constructed of porous carbon. For high power density, high interfacial area between the electrodes is desirable. Therefore, a fluted BASE tube is selected, shown in Fig 1. The largest inside dimension of the tube, between the extremes of opposing lobes, is 0.04 m. The figure is drawn to scale. The cells are built with 0.21 m of electrochemically active height.

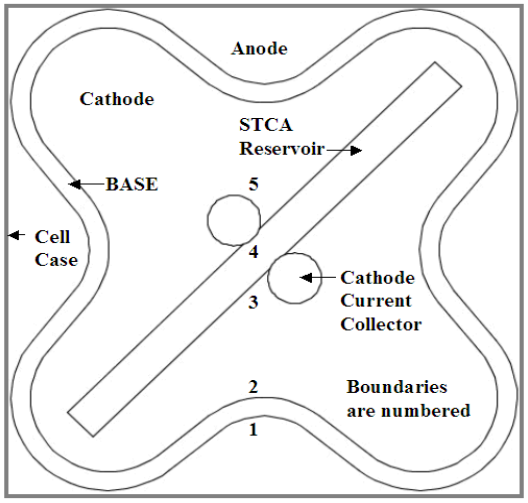

Figure 1. Cross-section of the sodium | metal chloride cell. The anode occupies the volume between the fluted BASE tube and the steel case. The cathode is fabricated in the fluted BASE tube.

The reversible cell reaction is

$$2\,Na + FeCl_2 \leftrightarrow 2\,NaCl + Fe \qquad [1]$$

Discharge occurs left to right, and charge right to left. During charge, sodium chloride, somewhat soluble in STCA, supplies chloride ions to the oxidation reaction at the iron surface. Ferrous chloride, nearly insoluble in 300°C STCA, crystallizes adjacent to the iron. Sodium ions transport through the BASE, and reduce to sodium in the anode. The iron powder serves as electrode and electronic pathway to the CC. The iron surface becomes passivated by formation of ferrous chloride during charging. Excessive charging could compromise the electronic pathway.

Control strategy design for hybrid propulsion systems requires simulation of the drive trains, including battery-operating characteristics, over a wide range of operating modes. Here we use

FEM analysis to simulate sodium | ferrous chloride cell operation.

2. Governing Equations

A 2D electrochemical cell model has been constructed with three subdomains: the BASE tube, the STCA reservoir, and the porous electrode, using Fig 1 geometry. The anode and the cathode CC are not explicitly modeled. The model has been used to characterize 300°C, isothermal, constant-current discharge. Symbols are defined in the Appendix. Boundary conditions (BCs) are referred to the numbered boundaries in Fig 1.

2.1 β" Alumina Solid Electrolyte Separator

BASE is modeled as a solid conductor, with sodium ion charge carriers, using the DC conduction continuity equation.

$$\vec{\nabla} \cdot \kappa_B \vec{\nabla} \varphi_2 = 0 \qquad [2]$$

At boundary 1[1]:

$$\varphi_2 = \frac{-\vec{i}_2 \cdot \vec{n}}{i_{0N}} \frac{RT}{F} \qquad [3]$$

Eq 3 models over-potential associated with the exchange current density at the sodium anode, using the linearized Butler-Volmer equation[1]. The BC at boundary 2 is current continuity.

2.2 STCA Reservoir

The cathode solids shrink *ca* 15% from the discharged to the fully charged state, due to consumption of solid NaCl. During charge, STCA transfers to the porous cathode from the reservoir, and during discharge, STCA transfers out. The porous structure suspends molten STCA by capillary action, preventing pooling at the cathode base. Because the reservoir never saturates with SCTA, we assume discontinuous distribution of the STCA phase in the reservoir; transport in the SCTA phase is neglected. The continuous, carbon structure supports electronic conduction. Current density, as defined for this phase, is superficial. *I.e.*, current density is defined over the total cross-section, rather than the cross-section of the carbon phase. Conductivity σ_C = 635 S/m is defined accordingly.

$$\vec{\nabla} \cdot \sigma_C \vec{\nabla} \varphi_1 = 0 \qquad [4]$$

The BC at boundary 3, between the iron network of the porous cathode and the carbon network of the reservoir, is current continuity. At boundary 4, we assume uniform current flux.

$$\vec{i}_1 \cdot \vec{n} = \frac{I}{2\pi d_C} \qquad [5]$$

In the present example, cell current I = -38.7 A/m of active cell height.

2.3 Porous Cathode

The porous cathode comprises a conductive network of iron particles, partially covered with $FeCl_2$ crystals, depending on the depth of discharge (DoD). Interspersed among the Fe/$FeCl_2$ network are NaCl crystals. The interconnecting pores are filled with electrolyte, modeled as a fully dissociated binary solution of STCA and NaCl. This model is applicable for basic (NaCl-saturated) to mildly acidic compositions[2]. Transport phenomena in the electrolyte include ionic charge migration, diffusion and convection. As defined for this phase, electronic and ionic current densities, convective velocity, and diffusive flux are superficial; the diffusion coefficient and the ionic and electronic conductivities are defined accordingly.

The dependent field variables are φ_1, φ_2, ε_m, ε_s, ε_p, x_A, and $\vec{v}_m$. These are electric field potentials in the iron and electrolyte phases; volume fractions of iron, $FeCl_2$, and NaCl; mole fraction of STCA in the electrolyte, and molar-average, electrolyte velocity; respectively.

In addition to PDEs and BCs, rate expressions are required for the two reactions that occur at the pore-wall interface, NaCl phase transfer and Fe/$FeCl_2$ REDOX.

<u>*NaCl Phase Transfer*</u>. NaCl is produced and consumed via Eq 1. The solid NaCl phase grows or shrinks in volume, via mass transfer from or to the electrolyte.

$$Na^+ + Cl^- \Leftrightarrow NaCl(solid) \qquad [6]$$

The following mass-transfer rate expression, is a modification of that in reference 1.

$$R_p = k_p \left(\frac{1 - x_A}{\overline{V}_e^2} - K_{sp} \right) \frac{\varepsilon_p}{\widetilde{\varepsilon}_p} \qquad [7]$$

The solubility product K_{sp} is the product of the sodium ion and chloride ion concentrations in NaCl-saturated STCA. Positive R_p is associated with precipitation. Electrolyte molar volume is:

$$\overline{V}_e = \frac{1}{\rho_e}\left[x_A M_A + (1 - x_A) M_B\right] \quad [8]$$

Eq 7 implicitly assumes that precipitation occurs predominantly by propagation.

The NaCl reference volume fraction is set to the average value at full discharge, 0.350. For the initial NaCl volume fraction, 0.010 is chosen. Had we used zero, the rate of precipitation, per Eq 7, would be zero throughout discharging.

Reduction/Oxidation. At the cathode:

$$2\,e^- + FeCl_2\,(solid) \leftrightarrow 2\,Cl^- + Fe\,(solid) \quad [9]$$

We use the following reaction rate expression, a modification of that in reference 1.

$$j = \frac{e^{\frac{\alpha_a F}{RT}\eta} - e^{\frac{-\alpha_c F}{RT}\eta}}{\frac{1}{i_0 \frac{a_m}{\widetilde{a}_s}\left(\frac{c_B}{\widetilde{c}_B}\right)^{2\beta}} + \frac{e^{\frac{-\alpha_c F}{RT}\eta}}{nFc_{r|q}}\left(\frac{1}{k_m \frac{a_m}{\widetilde{a}_s}} + \frac{1}{k_s \frac{a_s}{\widetilde{a}_s}}\right)} \quad [10]$$

Over-potential is:

$$\eta = \varphi_1 - \varphi_2 \quad [11]$$

The reference NaCl concentration is that of NaCl-saturated STCA. Oxidation is associated with positive over-potential η and transfer current density j. $FeCl_2$, in the form of a mobile species **r**, transfers between the electrolyte and the iron surface, and between the electrolyte and the $FeCl_2$ surface. Species **r**, assumed slightly soluble in the electrolyte, may be Na_2FeCl_4. Either the electron insertion reaction, or transfer of $FeCl_2$ between phases, can be rate limiting. Surface-area densities are estimated using:

$$\frac{a_m}{\widetilde{a}_m} = \left(\frac{\varepsilon_m - \varepsilon_{m|c}}{\widetilde{\varepsilon}_m - \varepsilon_{m|c}}\right)^{\frac{2}{3}}\left[1 - \left(\frac{\varepsilon_p + \varepsilon_s}{1 - \varepsilon_m}\right)^{\frac{2}{3}}\right] \quad [12]$$

$$\frac{a_s}{\widetilde{a}_s} = \left(\frac{\varepsilon_s}{\widetilde{\varepsilon}_s}\right)^{\frac{2}{3}} \quad [13]$$

The critical value of iron volume fraction $\varepsilon_{m|c}$ = 0.0665, is the value corresponding to passivation during charging. The iron and $FeCl_2$ reference volume fractions, 0.184 and 0.260, respectively, correspond to the fully charged state, which is the initial condition. This volume fraction of $FeCl_2$ corresponds to 7.88×10^5 coul/m of cell height, or 1.25×10^9 coul/m^3. For this example, constant-current discharging at –38.7 A/m, the full discharge time is 20,380 s (5.66 h).

The area-density reference values used in Eqs 12 and 13 are 5.52×10^5/m and 1.20×10^6/m, for iron and $FeCl_2$, respectively.

Solid Phase Mass Balances. Mass balances for iron, ferrous chloride and sodium chloride are:

$$\frac{\partial \varepsilon_m}{\partial t} = -\frac{j\hat{V}_m}{nF} \quad [14]$$

$$\frac{\partial \varepsilon_s}{\partial t} = \frac{j\hat{V}_s}{nF} \quad [15]$$

$$\frac{\partial \varepsilon_p}{\partial t} = R_p \hat{V}_p \quad [16]$$

Boundary conditions are not required.

Iron Phase Conduction. The iron network is modeled as a DC conductive medium.

$$\vec{\nabla} \cdot \sigma_{m|e} \vec{\nabla} \varphi_1 = j \quad [17]$$

To estimate effective conductivity of the iron network, the porous cathode is modeled as a Bruggeman asymmetric medium[3].

$$\sigma_{m|e} = \sigma_m \varepsilon_m^{3/2} \quad [18]$$

At boundary 3, the BC is current density continuity. At boundary 5, Eq 5 is the BC. At boundary 2, the insulation BC is appropriate.

$$\vec{n} \cdot \vec{i}_1 = 0 \quad [19]$$

Molten-Salt Phase Conduction. The continuity equation for DC conduction:

$$\vec{\nabla} \cdot \vec{i}_2 = j \quad [20]$$

Is combined with Ohm's law[4]:

$$\vec{i}_2 = -\kappa_{e|e} \vec{\nabla} \varphi_2 + \frac{\kappa_{e|e} RT}{F(1 - x_A)}\left(1 + \frac{d \ln(\gamma_A)}{d \ln(x_A)}\right)\vec{\nabla} x_A \quad [21]$$

The second term includes the diffusion potential. Effective conductivity is again estimated using the Bruggeman asymmetric-medium model:

$$\kappa_{e|e} = \kappa_e \varepsilon^{3/2} \quad [22]$$

Porosity ε is calculated as:

$$\varepsilon = 1 - \varepsilon_m - \varepsilon_s - \varepsilon_p \quad [23]$$

At boundary 2, the BC is current continuity. At boundaries 3 and 5, the BC

$$\vec{n}\cdot\vec{\nabla}\varphi_2 = 0 \qquad [24]$$

Taken together with the x_A BC at these two boundaries,

$$\vec{n}\cdot\vec{\nabla}x_A = 0 \qquad [25]$$

comprise the electrical insulation boundary condition.

Electrolyte Composition. Electrolyte composition is described by a single variable, STCA mole fraction x_A. The mass balance, written with respect to x_A, is

$$\varepsilon\frac{\partial x_A}{\partial t} = \frac{x_A}{c_T/2}R_p + \frac{x_A}{c_T/2}\frac{\vec{\nabla}\cdot\vec{i}_2}{F} + \left(\frac{1}{c_T}\frac{\vec{i}_2}{F} - \vec{v}_m\right)\cdot\vec{\nabla}x_A + \vec{\nabla}\cdot\left(D_{e|e}\vec{\nabla}x_A\right) - \frac{c_T}{2}\left(V_A - V_B\right)D_{e|e}\left(\vec{\nabla}x_A\right)^2 \qquad [26]$$

Similar to Eq 22:

$$D_{e|e} = D_e\varepsilon^{3/2} \qquad [27]$$

The total ion concentration is:

$$c_T = \frac{2\rho_e}{x_A M_A + \left(1-x_A\right)M_B} \qquad [28]$$

The NaCl concentration, as appears in Eq 10, is:

$$c_B = \left(1-x_A\right)\frac{c_T}{2} \qquad [29]$$

Molar volumes of the melt constituents are

$$V_A \equiv \frac{M_A}{\rho_e},\ V_B \equiv \frac{M_B}{\rho_e} \qquad [30]$$

At boundaries 2, 3 and 5, Eq 25 is the BC, assuring no mass diffusion across these boundaries. The initial condition for x_A is the NaCl-saturated value, 0.8972[1].

Velocity. Molar average velocity is defined as[4]:

$$\vec{v}_m = \frac{1}{c_T}\sum_i \vec{N}_i \qquad [31]$$

With summation over the three ionic species in the electrolyte, $AlCl4^-$, Cl^-, and Na^+. The volume continuity equation is[1]:

$$\vec{\nabla}\cdot\vec{v}_m = -\left(\hat{V}_m - \hat{V}_s + 2V_B\right)\frac{j}{2F} + \left(\hat{V}_p - V_B\right)R_p + \left(V_A - V_B\right)\vec{\nabla}\cdot\left(D_{e|e}\frac{c_T}{2}\vec{\nabla}x_A\right) + \vec{\nabla}\cdot\left(\frac{\vec{i}_2}{Fc_T}\right) \qquad [32]$$

Analogous to pressure in Darcy's law, we introduce a fictive velocity potential field p.

$$\vec{v}_m = -\vec{\nabla}p \qquad [33]$$

Permeability and viscosity are not required in this case, where convection is driven by geometry change, not pressure. All ionic species exhibit zero flux across boundary 5.

$$\vec{n}\cdot\vec{v}_m = -\vec{n}\cdot\vec{\nabla}p = 0 \qquad [36]$$

Only Na^+ has non-zero flux across boundary 2.

$$\vec{n}\cdot\left(\vec{v}_m + \frac{\vec{i}_2}{Fc_T}\right) = \vec{n}\cdot\left(-\vec{\nabla}p + \frac{\vec{i}_2}{Fc_T}\right) = 0 \qquad [37]$$

The boundary 3 BC is

$$p = 0 \qquad [38]$$

3. Method

All PDEs and boundary conditions were defined using the PDE, General Form in Comsol Multiphysics 3.4. The geometry was created from an imported CAD drawing. We did not make use of geometric symmetry to reduce DoFs in anticipation of future non-symmetric geometry modifications. We used a fixed mesh with 4180 triangular elements and 39,031 DoFs. UMFPACK was the solver, with time steps left free.

Unless otherwise noted, material parameters are those of reference 1.

4. Results and Discussion

Fig 2 presents surface maps of areal transfer current density, j/a_m, after 1000 (DoD = 4.9%) and 12,000 s (58.9%) discharges. Scales, in A/m^2, differ between panels. At 58.9% DoD, a crest of low j/a_m has translated inward, putting separation between the crest and the BASE; also, the j/a_m crest is broader and reduced in magnitude. Superimposed $\boldsymbol{i_1}$ arrow maps show electronic current density direction and magnitude. $\boldsymbol{i_1}$ is directed from the j/a_m crest toward the CC. $\boldsymbol{i_1}$ vanishes between the BASE and the crest, a region where current is mostly ionic.

Fig 3 presents surface maps of NaCl mole fraction x_B, relative to the reference value for NaCl-saturated STCA. Values greater than 1

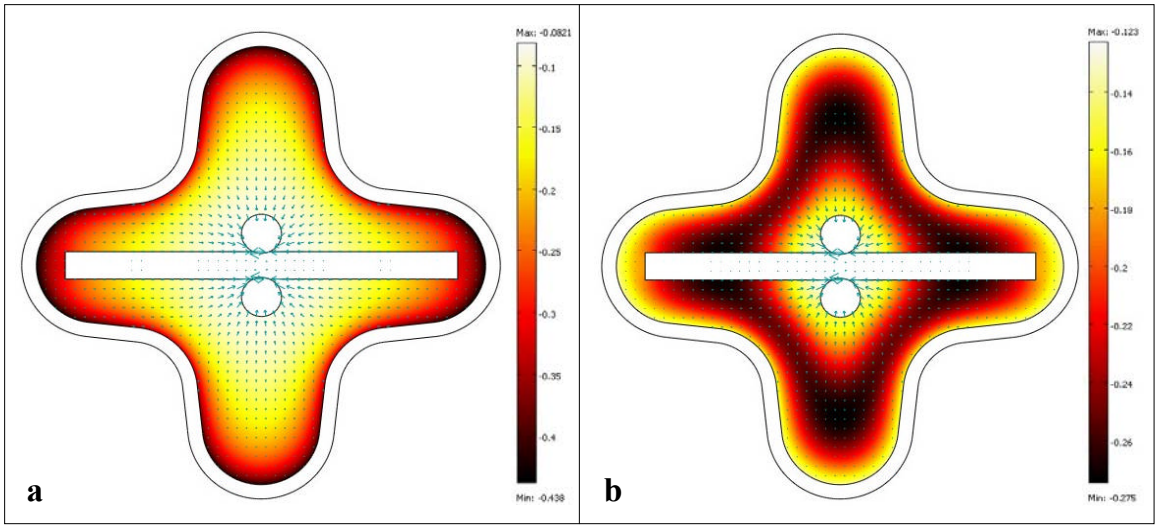

Figure 2. j/a_m (color map) and $\vec{i}_1$ (arrow map) at (a) 4.9% and (b) 58.9% DoD. Scales are different between panels.

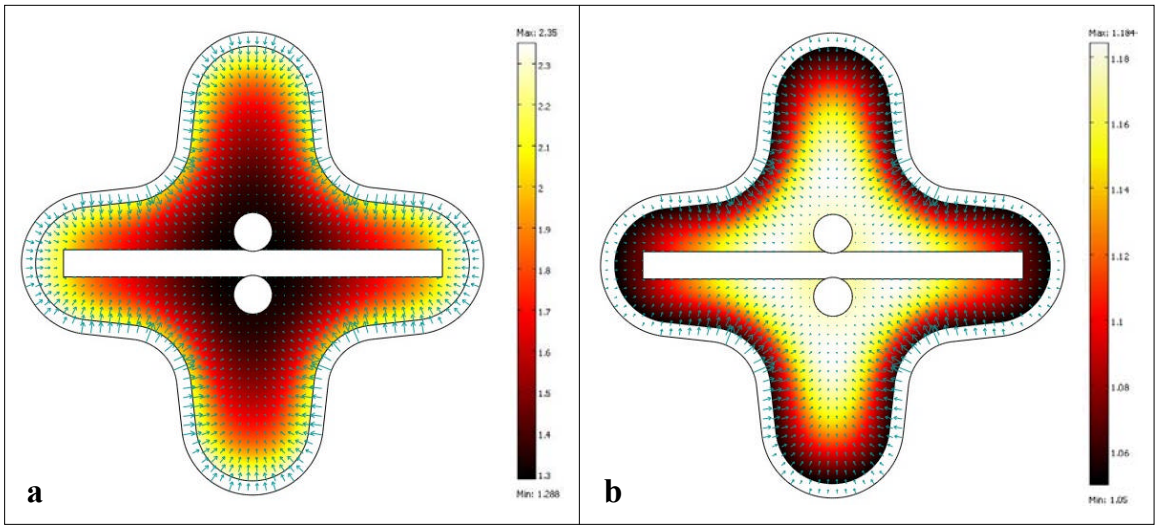

Figure 3. $x_B/\widetilde{x}_B$ (color map) and $\vec{i}_2$ (arrow map) after (a) 4.9% and (b) 58.9% DoD. Scales differ between panels.

indicate super-saturation. At 4.9% DoD, little NaCl precipitation has occurred, and high super-saturation is predicted, especially near the BASE, where most discharge has occurred. At 58.9% DoD, super-saturation is reduced. Near the BASE separator, behind the crest, x_B has nearly returned to equilibrium. Superimposed $\boldsymbol{i_2}$ arrow maps show ionic current density. $\boldsymbol{i_2}$ tends to zero in front of the reaction front, where current is predominantly electronic. At 4.8% DoD, ionic current supplied from the anode is essentially uniform around the perimeter of the cathode. At 58.9% DoD, ionic current is supplied primarily from the concave surfaces between the separator's flutes, causing "hot spots" in the BASE.

Fig 4 shows ε_s and $\boldsymbol{v_m}$. At 58.9% DoD, $FeCl_2$ is depleted adjacent to the BASE separator, driving the reaction crest inward. Near the separator, $\boldsymbol{v_m}$ is directed toward the reaction crest, due to Na^+ fluxing from the anode. Inside

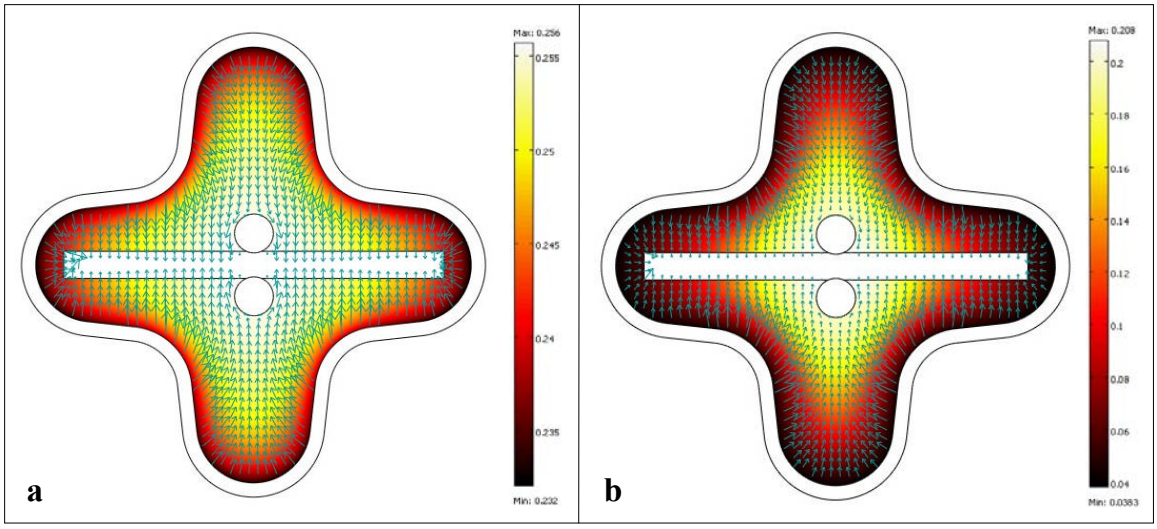

Figure 4. ε_s (color map) and $\vec{v}_m$ (arrow map) after (a) 4.9% and (b) 58.9% DoD. Scales are different between panels.

of the crest, $\boldsymbol{v_m}$ is directed toward the reservoir, as precipitation of NaCl displaces electrolyte.

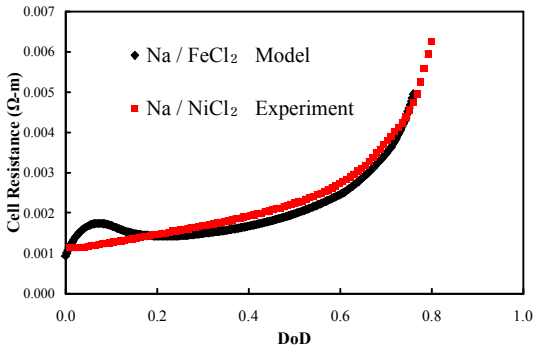

Figure 5. Cell resistance: model versus experiment.

Fig 5 compares cell resistance versus DoD from the model with experiment. Resistance has units of Ω-m of cell height. The cell geometry and temperature were the same, but the cathode was nickel/$NiCl_2$, and current was –76.2 A/m. Na | $NiCl_2$ and Na | $FeCl_2$ cells behave similarly. Model cell resistance was calculated:

$$R_c = \left(\langle \varphi_1 \rangle \Big|_{\substack{current \\ collector}} + \langle \Delta U \rangle \Big|_{\substack{BASE \\ separator}} \right) \Big/ I \qquad [39]$$

Where ΔU is equilibrium potential deviation from the NaCl-saturated STCA reference state. The Nernst equation is approximated:

$$\Delta U = -\frac{RT}{F} \ln \frac{x_B}{\tilde{x}_B} \qquad [40]$$

Eq 39 averages over the CC and BASE perimeters. Agreement is acceptable, except at the discharge onset. At onset, Eq. 7, describing NaCl precipitation, under-estimates the rate.

5. Conclusion

A mathematical model for operation of a high-temperature sodium | metal chloride cell is presented, along with FEM simulation. The model predicts increasing cell resistance during discharge, as the reaction front in the cathode moves away from the anode interface. Comparison with experiment, while satisfactory, suggests that reaction kinetics models for the pore-wall flux should be improved.

6. Appendix: List of Symbols

6.1 Roman

a_m	Iron surface area density (1/m)
$\tilde{a}_m$	Reference value for a_m (1/m)
a_s	$FeCl_2$ surface area density (1/m)
$\tilde{a}_s$	Reference value for a_s (1/m)
c_B	NaCl concentration (mole/m^3)

$\widetilde{c}_B$ Reference value for c_B (mole/m^3)

$c_{r|q}$ Equilibrium concentration of **r** (mole/m^3)

c_T Total ion concentration (mole/m^3)

D_e Binary melt diffusion coefficient (m^2/s)

$D_{e|e}$ Melt effective diffusion coefficient (m^2/s)

d_C Cathode CC diameter (m)

F Faraday number (A-s/mole)

I Cell current (A/m)

i_0 Equilibrium exchange current density at iron electrode (A/m^2)

i_{0N} Equilibrium exchange current density at sodium electrode (A/m^2)

$\vec{i}_1, \vec{i}_2$ Electronic and ionic current densities (A/m^2)

j Transfer current density (A/m^3)

K_{sp} Solubility product for NaCl in STCA (mole/m^3)^2

k_m **r** mass transfer coefficient at iron (m/s)

k_p NaCl mass-transfer coefficient (1/s)

k_s **r** mass transfer coefficient at $FeCl_2$ (m/s)

M_A Molar mass of STCA (kg/mole)

M_B Molar mass of NaCl (kg/mole)

$\vec{N}_i$ Superficial flux of ionic species i (mole/m^2-s)

n Number of electrons in Eq 9

$\vec{n}$ Outward-pointing unit normal vector

p Fictive pressure field (m^2/s)

R Gas constant (V-A/°K-mole)

R_c Cell resistance (Ω-m)

R_p Rate of NaCl phase change (mole/m^3-s)

T Temperature (°K)

ΔU Change in equilibrium potential (V)

V_A STCA melt molar volume (m^3/mole)

V_B NaCl melt molar volume (m^3/mole)

$\overline{V}_e$ Molar volume of electrolyte (m^3/mole)

$\hat{V}_m$ Molar volume of iron (m^3/mole)

$\hat{V}_p$ Molar volume of solid NaCl (m^3/mole)

$\hat{V}_s$ Molar volume of $FeCl_2$ (m^3/mole)

$\vec{v}_m$ Molar-average electrolyte velocity (m/s)

x_A STCA mole fraction in molten electrolyte

$\widetilde{x}_A$ Reference value for x_A

x_B NaCl mole fraction in molten electrolyte

$\widetilde{x}_B$ Reference value for x_B

6.2 Greek

α_a Anodic transfer coefficient

α_c Cathodic transfer coefficient

β Symmetry factor

γ_A STCA activity coefficient

ε Porosity

ε_m Iron volume fraction

$\widetilde{\varepsilon}_m$ Reference value for ε_m

$\varepsilon_{m|c}$ Critical passivation value for ε_m

ε_p Solid NaCl volume fraction

$\widetilde{\varepsilon}_p$ Reference value for ε_p

ε_s $FeCl_2$ volume fraction

$\widetilde{\varepsilon}_s$ Reference value for ε_s

η Over-potential in Eq 10 (V)

κ_B BASE ionic conductivity (S/m)

κ_e Electrolyte conductivity (S/m)

$\kappa_{e|e}$ Electrolyte effective conductivity (S/m)

ρ_e Density of electrolyte (kg/m^3)

σ_C Reservoir electronic conductivity (S/m)

σ_m Iron conductivity (S/m)

$\sigma_{m|e}$ Iron network effective conductivity (S/m)

φ_1 Electronic-media potential *vs* sodium (V)

φ_2 Ionic-media potential *vs* sodium (V)

7. References

1. M. Sudoh and J. Newman, Mathematical Modeling of the Sodium/Iron Chloride Battery, *J. Electrochem. Soc.*, **137**(3), 876-883 (1990).

2. L. G. Boxall, H.L. Jones and R. A. Osteryoung, Solvent Equilibria of $AlCl_3$-NaCl Melts, *J. Electrochem. Soc.*, **120**(2), 223-231 (1973).

3. D. S. McLachlan, M. Blaszkiewicz and R. E. Newnham, Electrical Resistivity of Composites, *J. Am. Ceram. Soc.*, **73**(8), 2187-2203 (1990).

4. R. Pollard and J. Newman, Transport Equations for a Mixture of Two Binary Molten Salts in a Porous Electrode, *J. Electrochem. Soc.*, **126**(10), 1713-1717 (1979).